Available online www.jsaer.com

***Journal of Scientific and Engineering Research*, 2019, 6(3):268-283**

Research Article

ISSN: 2394-2630
CODEN(USA): JSERBR

A Study of Flow Field in Low Swirl Injector

Baher A. Aboulkoll[1]*, Kamel A. Elshorbagy[2]

[1]Research Assistant, Alexandria University, Faculty of Engineering, Mech. Eng. Dept., Alexandria, 21544
[2]Professor, Alexandria University, Faculty of Engineering, Mech. Eng. Dept., Alexandria, 21544
* Corresponding Author, E-mail: baher.aboulkoll@gmail.com

Abstract Low Swirl Injector (LSI) is considered a promising technology for lean premixed combustion method. In recent years, this practice has been investigated experimentally and numerically.

A hypothesis is assumed in the present study that a combination of 3D simulation for LSI and 2D simulation for combustor computational domain could get better 2D simulation results with relatively low computational time compared with the 3D simulation for the entire combustor computational domain.

The goal of this study is to model the flow field of the Low Swirl Injector with non-reacting, 3D, Large Eddy Simulation, in order to get better values for the flow field, produced by the injector. These results are used as input data for 2D, non-reacting, RANS simulation using RSM for modeling the turbulence. The challenge is to obtain the best velocity profiles that would match the experimental data with lowest computational time.

Keywords 2D Non-reacting simulation, RANS, RSM, LSI

Nomenclature

K	Turbulent kinetic energy, (N.m/kg)
P_0	Inlet pressure, (Pa)
Re	Reynolds number, (ρvL/μ)
S	Swirl number (Dimensionless)
T	Time variable, (sec)
T_0	Inlet temperature, (K)
u’	Turbulence intensity,
U_0	Inlet velocity, (m/s)
x , y , z	Cartesian coordinates, (m)
μ	Viscosity, (kg/s.m)
ν	Kinematic viscosity, (m^2/s)
δ_{ij}	Kronecker delta
ρg_i	Body force, (N/m^3)
E	Eddy dissipation rate, (m^2/s^3)
ϕ	Any scalar
$\bar{\phi}, \phi'$	Mean and fluctuation of any scalar
$\tilde{\phi}, \phi''$	Favre mean and favre fluctuating part of any scalar
τ_{ij}	Stress tensor, (N/m^2)
i ,j ,k	Tensor coordinates
HSI	High swirl injector
LPM	Lean premixed
LSB	Low swirl burner

LSC	Low swirl combustor
LSI	Low swirl injector
RANS	Reynolds-Averaged-Navier-Stokes
RSM	Reynolds Stress Model

Introduction

In recent years, the necessity of clean combustion technology became more crucial urged by strict emission standards in industrial applications. LPM combustion became the most promising clean technology for practical systems. In Lean Premixed (LPM) combustion, the air and fuel are premixed upstream the combustor to avoid the formation of stoichiometric regions. The combustion zone is operated with excess air to reduce the flame temperature; consequently, thermal NOx is virtually eliminated [1]. Low Swirl Combustion is considered one of the most encouraging strategies for premixed combustion stabilization. The low swirl burner was initially proposed by Chan et al., [2] then developed mainly in the last decade. Low swirl combustion has been commercialized for industrial process heaters and is being employed in gas turbines [3]. "Fig. 1." shows the difference between the conventional LPM injector and low swirl injector.

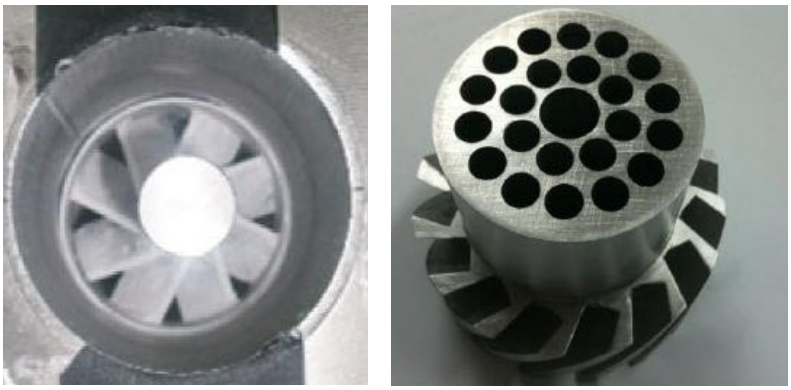

Figure 1: Left: High swirl injector, Right: Low swirl injector (Beerer, 2013)

The principle of low swirl burner (LSB) comes within the propagating nature of turbulent premixed flames. In LSBs, the "standing flame front" is accomplished by producing weak swirl which leads to a divergent downstream flow. Johnson's et al. [4] study clarified that unlike the High Swirl Injector (HSI) flames stabilized by high amounts of swirl, LSB flames do not depend on flow recirculation for stabilization. The main feature of the LSB is the distinctive design of swirl injector which produces slight swirl flow and facilitates downstream divergent flow where the flame front can be settled. The flow fields for both high and low swirl injector LPM gas turbines were compared by Johnson et al. [4]. The investigation performed by modifying a typical HSI gas turbine combustor to operate with LSI using particle image velocimetry. The results of LSI (S=0.5) were compared with those produced by HSI (S=0.73) which show that the LSI flow fields were entirely lacking of a large dominant recirculation zone. This is basically different than the strong and large recirculation regions that dominate flow fields of the HSI.

RANS simulation of combustion in a low swirl burner for the same configuration of Beerer's experiment [5] was conducted by Neumayer [6] in his simulations of premixed lean flames in a Low Swirl Burner. The results are compared with the corresponding experimental data. A 2D, axisymmetric, steady state, Reynolds-Averaged-Navier-Stokes (RANS) approach is used for the non-reacting simulations.

In this study the flow field of the LSI with non-reacting, 3D, LES model are conducted, in order to get better values for the flow field, produced by the injector. Those results are then used as input parameters for 2D, RANS simulation. The current study considers this technique that combines the 3D and 2D simulations for the sake of getting better quality results with respectively low computational time. There are three sets of simulations, the first set is a 2D RSM simulation of low swirl combustor model. The second one is a 3D LES of the LSI. The third set is enhanced 2D RSM simulation of LSC model using the output LES velocities of the LSI as input parameters for simulation.

Model Configuration

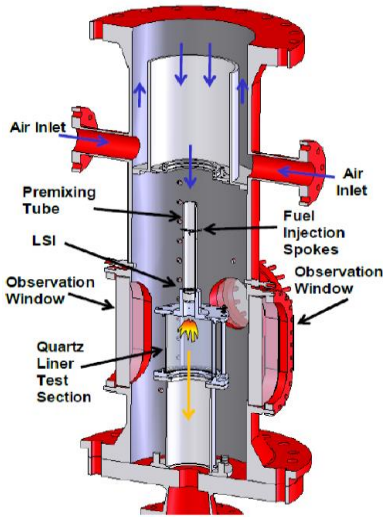

Figure 2: Cross section of the pressure vessel and combustor [5]

The current study is based on the experiment conducted by Beerer (2013) for numerical setup and results validation. Beerer's main experimental setup contains a premixer from which the fuel air mixture flows through the LSI, and then into the combustion chamber, which is divided into two parts, as shown in "Fig. 2". The first part is a quartz tube that is optically accessible by Laser Doppler Velocimetry measurements. The second part is a nontransparent steel tube.

Low Swirl Combustion

Cheng et al. [3] initially develop the LSI used in Beerer's experiment [5]. The flow enters the LSI is divided to swirled and unswirled flows as shown in "Fig. 3".

First, the swirled flow produced in the outer region by passing through 16 swirl vanes, with an outlet angle α_{vanes} = 37° to the axial direction. The swirled flow velocity has an axial and tangential components. Second, the unswirled flow passes through a perforated plate, which has 25 holes each of 2.6 mm diameter. The unswirled flow has only axial velocity component.

Figure 3: Low Swirl Injector. Right side inlet, left side outlet [5]

This is the main difference against HSI, which has a completely blocked center region, so all the incoming fluid become swirled. In the LSI, the supply of unswirled reactants through the center prevents the formation of a central recirculation zone and support the flow divergence [3]. As the incoming flow is divided into swirled flow through the swirler vanes and unswirled flow through the perforated plate, changing the mass flow split ratio influences the divergence rate and therefore the flame position.

Swirl can be indicated by the Swirl number S, representing the ratio of azimuthal momentum of the flow to the axial momentum. For the LSI the Swirl Number S formula can be found in Cheng et al., [3] as:

$$S = \frac{2}{3} tan\ (\alpha_{vanes}) \frac{1-R^3}{1-R^2+[m_{LSI}^2\left(\frac{1}{R^2}-1\right)^2]R^2} \quad (1)$$

$$Where\ R = \frac{R_C}{R_0}\text{, and } m_{LSI} = \frac{\dot{m}_C}{\dot{m}_S}$$

Where α_{vanes} is the swirl angle, R the ratio of the center channel radius, R_C to injector radius, R_0 and m_{LSI} the mass flow ratio (the mass flow through the center channel $\dot{m}_C$ to the mass flow through the swirl annulus $\dot{m}_S$).
In HSI, strong recirculation zones are present in the outer regions of the combustion chamber, as well as a recirculation zone in the center of the flow field [6]. In those recirculation zones, hot reaction products, including radicals are transported back upstream, where they ignite the unburned fuel air mixture. With this effect, the flame is stabilized close to the HSI.
In LSI the axial momentum is greater than the azimuthal momentum, which results in swirl numbers smaller than unity. The calculated swirl number in Beerer's [5] research is S = 0.5.
When the flow enters the combustion chamber, there is an increase in diameter, called sudden expansion. The radial momentum of the swirl makes the outer and the inner flow diverge. In accord with the conservation of mass law, the mean axial velocity decreases with distance away from the sudden expansion. Close to the centerline, the velocity decay is linear. When the flow from the injector enters the combustion chamber, there is also a shear layer formed, between the incoming flow and the fluid that is already in the combustion chamber.

Numerical Approach

Beerer's experiment is first modeled as a 2D model. The the low swirl injector is then modeled as a 3D model, studying the flow field, to get better values of velocity output. Finally those results of velocities are used as input data for the 2D model for the sake of enhancement the data quality.

Turbulence Modeling

Up to date, there is no sufficient Reynolds Stress Modeling (RSM) for the turbulence modeling of the LSI. The current study is a trial to fill the gap. All simulations are conducted using the software ANSYS Fluent, version 16.0.

Reynolds Stress Turbulence Model

The Reynolds stress model (RSM) [7-9] is the most elaborate type of RANS turbulence model that ANSYS Fluent provides. Abandoning the isotropic eddy-viscosity hypothesis, the RSM closes the Reynolds-averaged Navier-Stokes equations by solving transport equations for the Reynolds stresses, together with an equation for the dissipation rate. This means that five additional transport equations are required in 2D flows, in comparison to seven additional transport equations solved in 3D.
Since the RSM accounts for the effects of streamline curvature, swirl, rotation, and rapid changes in strain rate in a more rigorous manner than one-equation and two-equation models, so it has greater a potential to result in accurate predictions for complex flows.
The RSM might not always yield results that are clearly superior to the simpler models in all classes of flows to warrant the additional computational expense. However, use of RSM is a must when the flow features of interest are the result of anisotropy in the Reynolds stresses. Among the examples are cyclone flows and highly swirling flows in combustors.
The exact form of the Reynolds stress transport equations may be derived by taking moments of the exact momentum equation. This is a process wherein the exact momentum equations for the fluctuations are multiplied by the fluctuating velocities and averaged, the product is then being Reynolds-averaged. Unfortunately, several of the terms in the exact equation are unknown and modeling assumptions are required in order to close the equations. The Reynolds stress transport equations are thus set as:

$$\frac{\partial}{\partial t}\left(\rho\overline{u'_\iota u'_J}\right) + \frac{\partial}{\partial x_k}\left(\rho\bar{u}_k\overline{u'_\iota u'_J}\right) = P_{ij} + F_{ij} + D_{T,ij} + \phi_{ij} - \varepsilon_{ij} \quad (2)$$

Where

$$P_{ij} = \overline{u'_\iota u'_k}\frac{\partial u_j}{\partial x_k} + \overline{u'_J u'_k}\frac{\partial u_i}{\partial x_k} \quad (3)$$

And

$$F_{ij} = -2\Omega_k\left(\overline{u'_J u'_m}\varepsilon_{ikm} + \overline{u'_\iota u'_m}\varepsilon_{jkm}\right) \quad (4)$$

And for turbulent diffusion can simplified in ANSYS Fluent to use a scalar turbulent diffusivity as follows [10]:

$$D_{T,ij} = \frac{\partial}{\partial x_k}\left(\frac{\mu_t}{\sigma_k}\frac{\partial \overline{u_i' u_j'}}{\partial x_k}\right) \quad (5)$$

The turbulent viscosity, μ_t is computed using

$$\mu_t = \rho C_\mu \frac{k^2}{\varepsilon} \qquad \text{Where } C_\mu = 0.09.$$

Lien and Leschziner [10] derived a value of $\sigma_k = 0.82$ by applying the generalized gradient diffusion model, "Eq. (5)." to the case of a planar homogeneous shear flow. Note that this value of σ_k is different from that in the standard and realizable $k-\varepsilon$ models, in which $\sigma_k = 1.0$.

The classical approach to modeling ϕ_{ij} uses the following decomposition:

$$\phi_{ij} = \phi_{ij,1} + \phi_{ij,2} + \phi_{ij,w} \quad (6)$$

Where $\phi_{ij,1}$ is the slow pressure-strain term, also known as the return-to-isotropy term, $\phi_{ij,2}$ is called the rapid pressure-strain term, and $\phi_{ij,w}$ is the wall-reflection term.

The dissipation tensor, ε_{ij} is modeled as

$$\varepsilon_{ij} = \frac{2}{3}\delta_{ij}(\rho\varepsilon + Y_M) \quad (7)$$

Where $Y_M = 2\rho\varepsilon M_t^2$ is an additional "dilatation dissipation" term according to the model by Sarkar [11].

Large Eddy Simulation (LES)

Instead of solving all of the eddies, large eddy simulation addresses modeling large ones. LES puts a cut-off wave number, k_C, and solves the scales whose frequency wave number, k, is lower than the k_C. Scales whose frequencies higher than k_C are modeled. These are called subgrid scales and need to be treated carefully since they confine the conservation. Also the quality of the solution is highly dependent to the effects of small scales. In a flow, the large scales contain the most of the conserved properties.

Finite Volume Method – Pressure Based Approach

The pressure-based solver employs an algorithm which belongs to a general class of methods called the projection method [8]. In the projection method, the constraint of mass conservation (continuity) of the velocity field is achieved by solving a pressure (or pressure correction) equation. The pressure equation is derived from the continuity and the momentum equations in such a way that the velocity field, corrected by the pressure, satisfies the continuity.

2D Numerical Domain

The model configuration, was introduced by Beerer [5] then numerically investigated by Neumayer [6]. In this study, the same model configuration is modeled as a non-reacting, 2D axisymmetric setup, due to limited computational resources. Steady state, RANS simulations are conducted. "Fig. 4." demonstrates the numerical domain constructed for the present case which commences at downstream the swirler and extends to the outlet of the combustor.

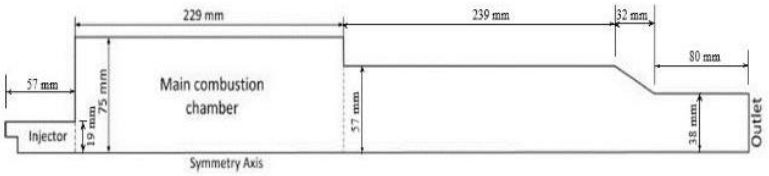

Figure 4: Numerical Domain of Low Swirl Combustor

3D Numerical Domain

"Figure 5." demonstrates the numerical domain constructed for the present model for the flow field of the Low Swirl Injector with non-reacting, 3D, LES, in order to get better values for the outlet velocities, produced by the injector. Those results are then used as input data for 2D, non-reacting, RANS simulation.

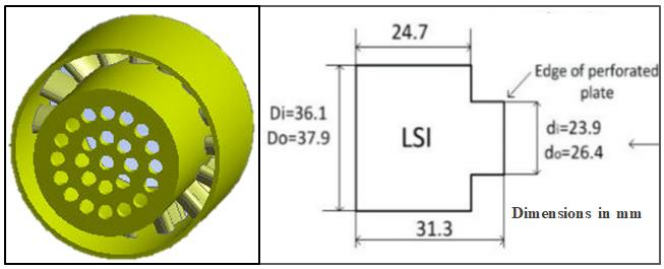

Figure 5: Numerical Domain of Low Swirl Injector

2D Boundary Conditions

For modeling the Low Swirl Injector (LSI) two mass flow inlets are used.

The perforated plate is modeled with a velocity vector, consisting only of an axial component. The annulus, including the swirl vanes is modeled using a velocity vector with both an axial and a tangential components.

The total mass flow rate of the fuel-air mixture in the experiments is known, but the flow split ratio through the LSI is unknown.

According to Neumayer [6], and based on Bernoulli's energy conservation equation for streamlines in incompressible flows, the mass flow split for the cold flow simulations is conducted. The mass flow through a nozzle is given by

$$\dot{m} = A_{eff}\sqrt{2\rho\Delta p_{LSI}} \quad (8)$$

Where ρ is the density of air and Δp_{LSI} = 13.1kPa is the pressure loss over the Low Swirl Injector, measured in the Beerer's experiment for cold flow at 4 atmospheric pressure. The effective area is calculated as:

$$A_{eff} = C_{loss}A_{geo} \quad (9)$$

Where A_{geo} is the geometric area. The Bernoulli approach calculation is an estimate to determine an initial value for the simulations. Therefore the loss coefficient C_{loss} is set to unity for both inlets.

$$\dot{m} = A_{geo}\sqrt{2\rho\Delta p_{LSI}} \quad (10)$$

For the perforated plate, the geometric area is determined as the number of holes, N_{holes} multiplied by the area of one hole, A_{hole}.

$$A_C = N_{holes}A_{hole} \quad (11)$$

For the swirler inlet, the geometric area is calculated as the area of the annulus A_{ann} minus the area blocked by the thickness of the swirl vanes, i.e. number of vanes N_{vanes} multiplied with the cross-sectional area of one vane A_{vane}.

$$A_S = A_{ann} - N_{vanes}A_{vane} \quad (12)$$

The calculated mass flow through the perforated plate inlet is thus

$\dot{m}_P = A_C\sqrt{2\rho\Delta p_{LSI}}$ = 0.0379 kg /s

And through the swirl inlet is

$\dot{m}_S = A_S\sqrt{2\rho\Delta p_{LSI}}$ = 0.1135 kg /s

The total mass flow rate according to the Bernoulli's approach calculation is 0.152 kg /s for cold flow, which is smaller than the total mass flow rate of (0.167 to 0.172 kg /s), measured with a mass flow meter during Beerer's experiment. The fractions of the total mass flow rate are calculated as:

$$F_C = \frac{\dot{m}_P}{\dot{m}_P + \dot{m}_S} = 0.25 \text{ and } F_S = \frac{\dot{m}_S}{\dot{m}_p + \dot{m}_S} = 0.75$$

In order to get a well-posed simulation setup, the exhaust outlet is modeled with a pressure outlet condition.

As the flow in the combustion chamber is viscid, all the walls are implemented as "nonslip walls".

To set the turbulence parameters of the flow at the mass flow inlets, it is intended to specify a turbulent length scale l_t and a turbulent intensity, which is defined as u'/U_0. For the perforated plate inlet, l_t is specified as the diameter of the holes in the plate. For the swirl inlet, l_t equals the gap height of the annulus.

Pressure based, 2-dimensional, axisymmetric simulations including swirl are conducted.

To calculate the density of air, the incompressible ideal gas model is considered.

A more sophisticated way of modeling turbulence is the RSM, which considers the anisotropy of the Reynolds Stress Tensor. One equation for each component of the Reynolds Stress Tensor is solved.
To resolve the boundary layers on the walls, the "enhanced wall treatment" is chosen. For the pressure velocity coupling the SIMPLE solver is used.
The Spatial Discretization method is set to Second Order for all variables. For the pressure solver, the PRESTO method is chosen; the Fluent User's Guide suggests this method for strongly swirling flows.

3D Boundary Conditions

For modeling the Low Swirl Injector mass flow inlet is used.
To set the turbulence parameters of the flow at the mass flow inlet, a turbulent hydraulic diameter is specified.
In order to get a well-posed simulation setup, the exhaust outlet is modeled with a pressure outlet condition.
As the flow in the combustion chamber is viscid, all the walls are implemented as "nonslip walls".
Pressure based, 3D, LES are conducted. To calculate the density of air, the incompressible ideal gas model is chosen, as the Mach-numbers at the inlets are smaller than 0.25.
For the pressure velocity coupling the SIMPLE solver is used. The Spatial Discretization method is set to Bounded Central Differencing for all variables. This is recommended for large eddy simulation by Fluent User's Guide. For the pressure solver, the PRESTO method is considered, as the Fluent User's Guide suggests this method for strongly swirling flows. Temporal Discretization method is set to Bounded Second Order Implicits.

2D Mesh Generation

Quadrilateral structured mesh, with 1mm element length in both spatial directions is identified as a base model. For the 1st refinement, the element is divided into two halves in both spatial directions in the first third of the domain (green area), as shown in "Fig.6.". For the 2nd and 3rd refinement, the same method is repeated. Details of 2D mesh independent study are shown in "Fig.7.".

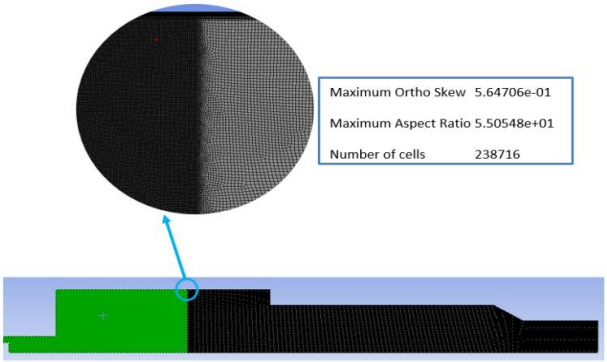

Figure 6: 2D Mesh for Computational domain (2nd refinement)

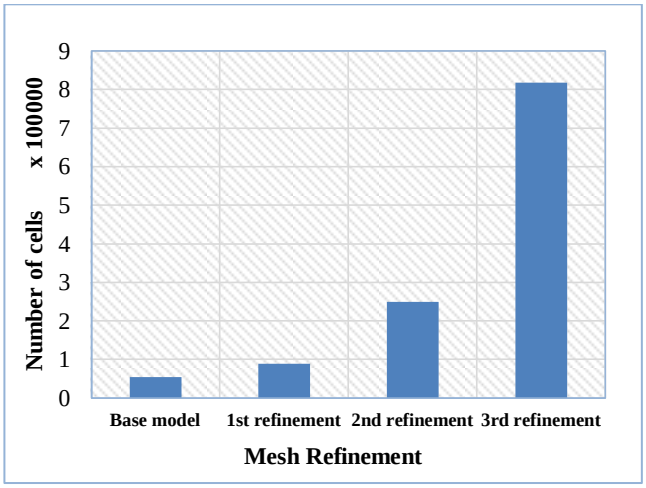

Figure 7: Details of 2D mesh independent study

3D Mesh Generation

"Figure 5." demonstrates the numerical domain constructed for the present model for the flow field of the Low Swirl Injector. For the mesh independent study six levels of hexahedral meshes are created. The first mesh, which is the most coarse one, has 71407 hexahedral elements. The finest mesh has nearly 3 million hexahedral elements. The details of meshes for mesh refinement are given in "Fig.8.". "Figure 9." shows the swirler computational domain and mesh refinements for the different mesh sizes.

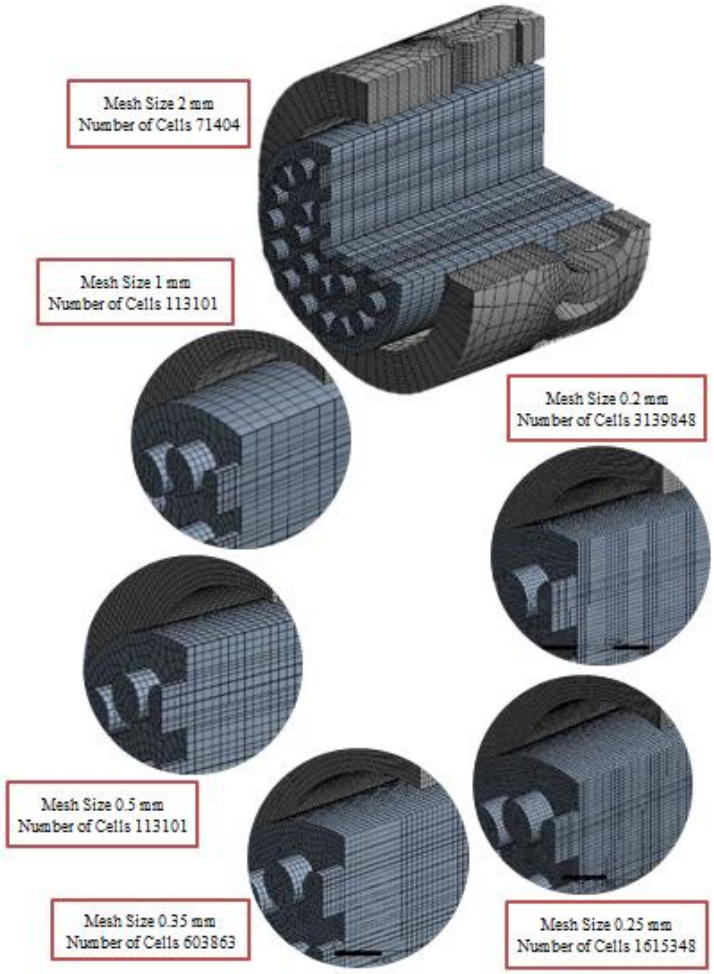

Figure 8: Detail of 3D mesh refinement of the swirler

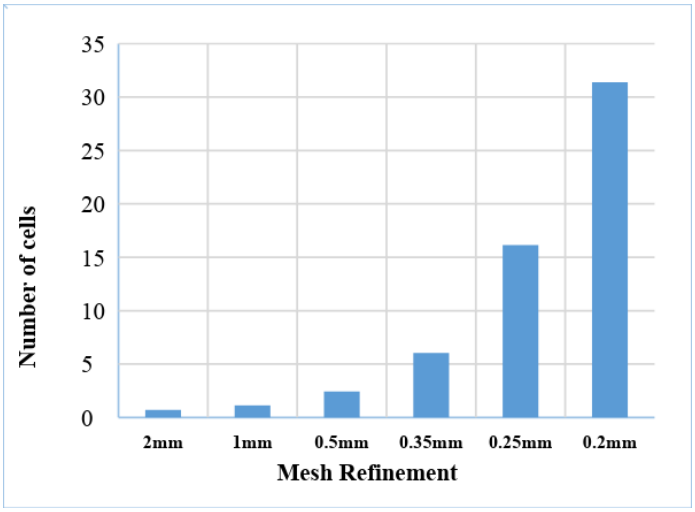

Figure 9: Details of Swirler mesh refinements in computational domain

Results

2D Mesh Independent study Results

Four different mesh sizes are used in conducting a mesh independent study comparing the axial velocity profile in radial direction. Results are given with the experimental data at a pressure of 1.1 atm. in "Fig. 10.", and at a pressure of 4 atm. as shown in Figure "Fig. 11".

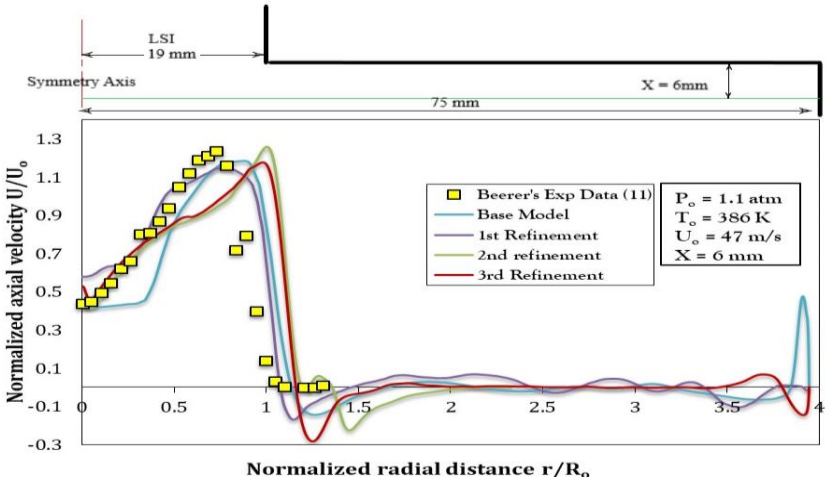

Figure 10: Mesh independent study (1.1 atm.)

From both figures the simulation shows that both 2nd and 3rd refinement data capture more details from the experimental data so for 2D calculations the 2nd refinement is chosen.

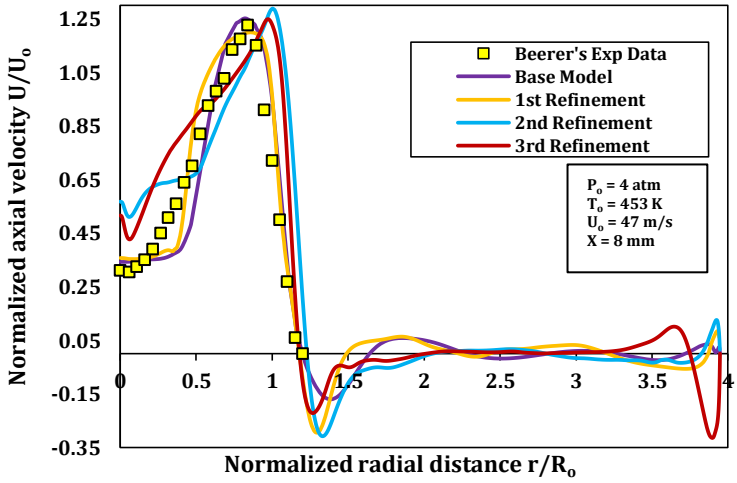

Figure 11: Mesh independent study (4 atm.)

3D Mesh Independent study Results

Six different mesh levels are used in conducting a mesh independent study comparing the axial velocity profile with axial line along the swirl axial direction (x=002, y=0.015m). As shown in "Fig.12." the mesh steps of 2mm and 1mm failed to catch the velocity profile, but the other four mesh steps show a tremendous good agreement in comparison with each other till 85% of the normalized swirler axial length. However, above 85% of this normalized swirler axial length, the more refiner is the mesh size the more details of the velocity profile captured. The results of mesh step sizes of 0.25mm and 0.2mm are almost identical, so the mesh step size of 0.25mm is considered suitable for the present case.

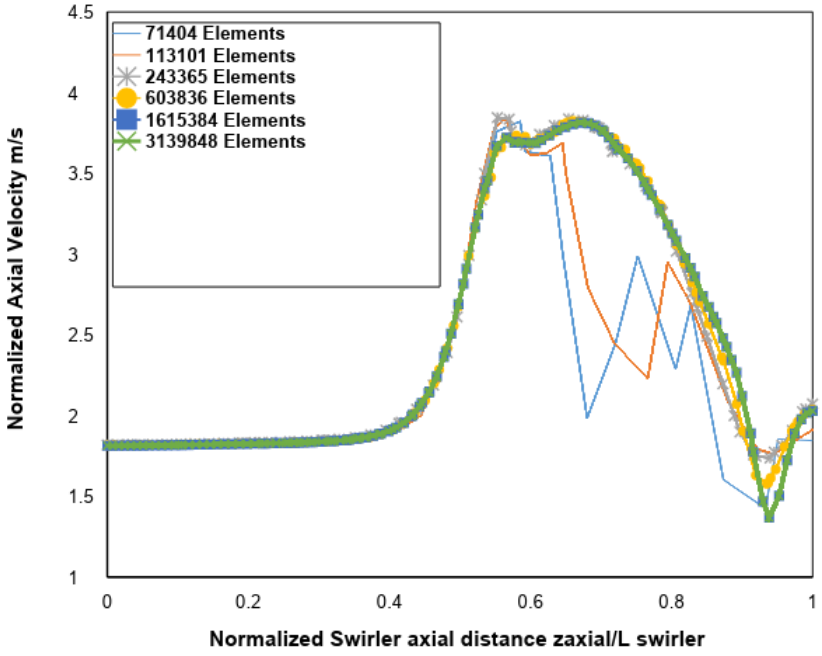

Figure 12: 3D Mesh refinement study results

The mean velocities downstream the swirler vanes are determined to be used as input parameters for the 2D enhanced.

2D Simulation Results

"Figure 13." shows the profile of normalized axial velocity in radial direction for different flow angles at operating pressure = 1.1 atm., measured at 6mm downstream the sudden expansion. The injector radius R_0 = 19mm and the average velocity in injector U_0 = 47m/s. A set of simulations at different flow angles are obtained because in a lot of applications of the low swirl injector the flow angle does not perfectly follow the vane angle. For example Strahman [12], reported that the actual swirl number calculated at different locations by integrating numerically the mean three-component velocity field, was greater than the value of computed geometric swirl number based on flow inputs due to the fact that the exit angle of the flow when it leaves the swirler was not the same as the exit angle of the vanes of the swirler. Also Graham [13], mentioned that the deviation of flow relative to vane angle changed with swirler geometry, especially the exit vane angle of the low swirl injector. To investigate this behavior a flow angle of 37^o which is the same angle of the vanes is simulated among other three angles. The results in "Fig. 13." shows a small deflection in flow angle. The best matched flow angle is 35^o.

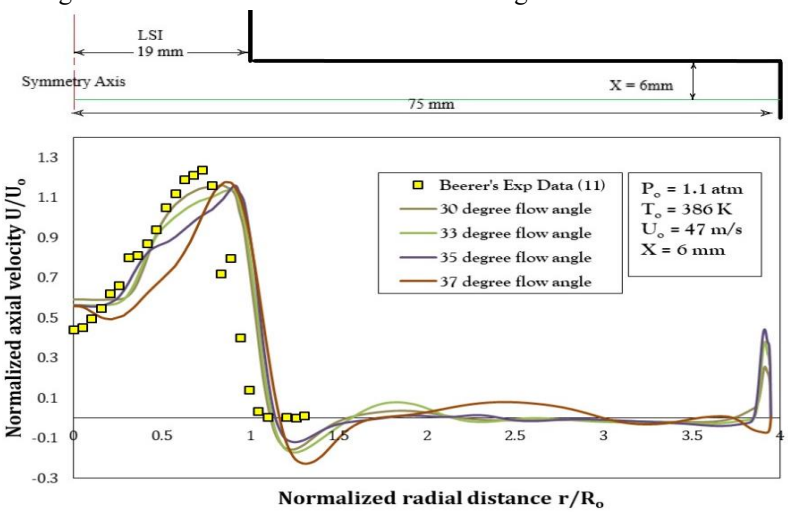

Figure 13: Axial velocity profile in radial direction for different flow angles

"Figure 14." shows the normalized axial velocity profile in radial direction for different flow split ratios at operating pressure = 1.1 atm., measured at 6mm downstream the sudden expansion. The injector radius R_0 = 19mm and average velocity U_0 = 47m/s. The shown set of simulations are considered to identify the flow split ratios of LSI because it may differ from the calculated value by Bernoulli's equation. The flow split ratio gained its importance from its direct effect, beside the perforated plate geometry, on the swirl number.

Littlejohn et al. (2010) investigated the effect of the flow split by varying the blockage ratio of the perforated plate on Solar Turbine's T70 SoLoNox injector. Also, Cheng et al. (2001) studied the effect of perforated plate configuration on flow split ratio to balance the flow between the swirled and unswirled flows. In "Fig.14." flow ratio of 1:3, which is the same as the calculated value, is simulated among other three flow ratios. The figure shows that ratio of best agreement with experimental is the flow ratio of 1:3.5.

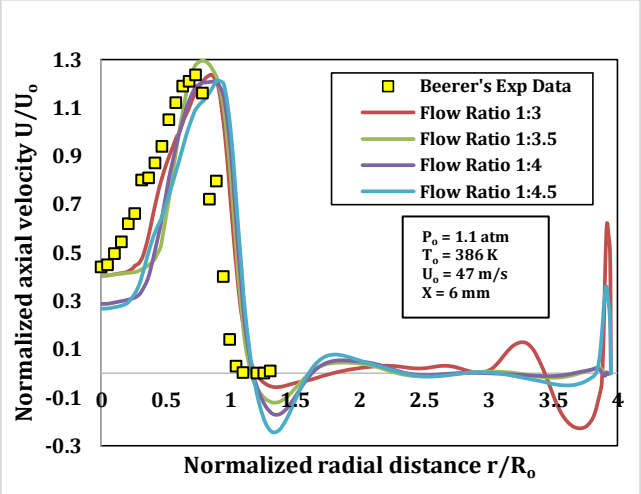

Figure 14: Axial velocity profile in radial direction for different flow ratios

"Figure 15." shows the normalized axial velocity profile in radial direction for a flow angle of 35 degree and 1:3.5 flow split ratio between the perforated inlet and swirl inlet. The simulated data are compared with both experimental data of Beerer [5] at 1.1 atm. and numerical results of Neumayer (2013) for the same pressure.

The simulations are made at 6mm downstream the sudden expansion for injector radius R_0 = 19mm and average velocity U_0 = 47m/s. The figure shows more agreement with Beerer's experimental data (2013) in comparison to Neumayer's Simulation [6] especially within the ranges (0 to 0.5) and (1.2 to 1.3) of normalized radial distance. This could be attributed to the present good reached mesh refinement. However, for the range of (0.55 to 1.1) the simulation results show disagreement with experimental data. This could be due to the mesh of this area that may need more refinement, which is sought to be extension for the present work.

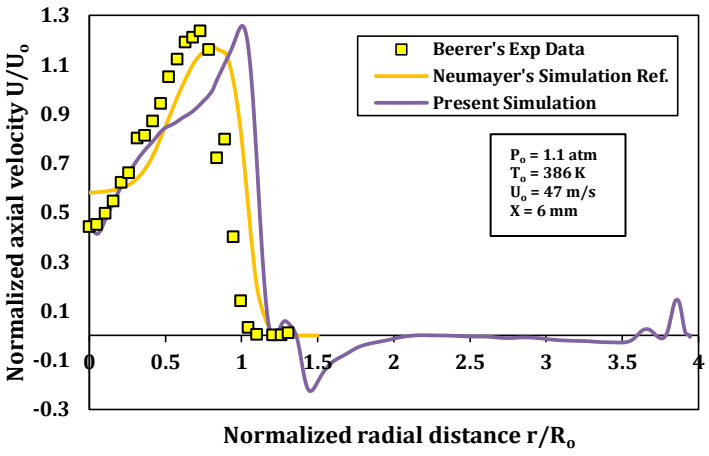

Figure 15: 2D simulation data (1.1 atm.)

"Figure 16." shows the normalized axial velocity profile in radial direction for flow angle of 35 degrees and 1:3.5 flow split ratio between the perforated inlet and swirl inlet. In addition, plotted in the figure, the axial velocity profile in radial direction obtained by Beerer [5] at 8mm downstream the sudden expansion. (injector radius R_0 = 19mm, average velocity in injector U_0 = 47m/s). The figure shows that present simulation data carries better similarity with Beerer's experimental data in comparison with Neumayer's simulation [6], especially within the range (0 to 0.5) of normalized radial distance. That is apparently due to a rather better mesh refinement.

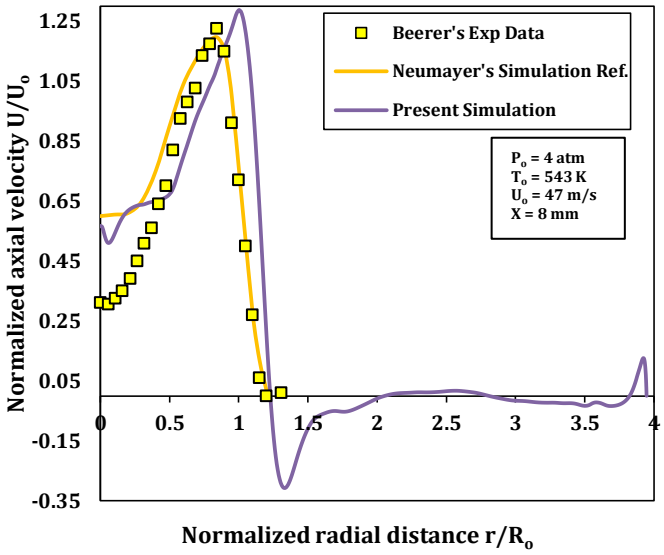

Figure 16: 2D simulation data (4 atm.)

"Figure 17." shows the axial velocity variation along the centerline of swirler after the sudden enlargement for flow angle of 35 degrees and 1:3.5 flow split ratio. The operating pressure is 8.1 atm., injector radius R_0 = 19mm and the average velocity in injector U_0 = 24.8 m/s.

The simulated data is compared only with Beerer's experimental data [5]. Neumayer's Simulation [6] is not included because the numerical data inputs do not match. The present simulation data hardly follows qualitatively the experimental data, apparently the mesh need more refinement in the area of high swirling after the sudden expansion.

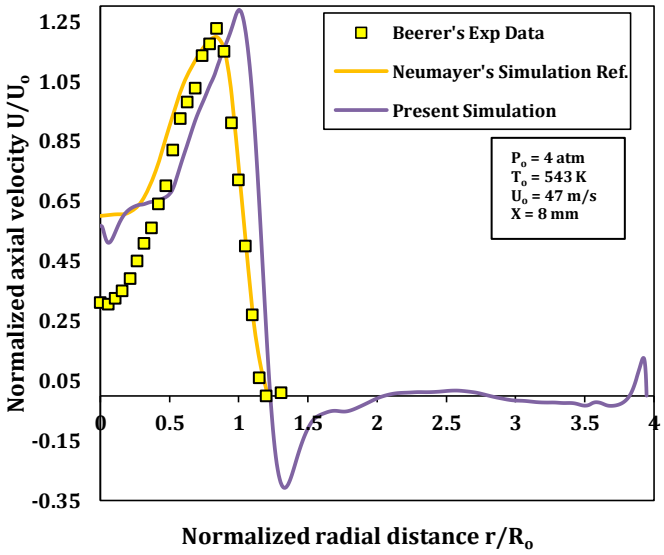

Figure 17: 2D simulation Data of axial velocity variation along the centerline of swirler

"Figure 18." shows the turbulence intensity profile in radial direction, measured by Beerer [5] at 8 mm downstream the sudden expansion, for flow angle of 35 degrees and 1:3.5 flow split ratio. The operating pressure is 4 atm., injector radius R_0 = 19 mm and average velocity in injector is $U_{0=}$ 47m/s. The simulation data is compared to this experimental data and Neumayer's Simulation [6] at the same operating conditions.

The present simulation data shows better match with the experimental data, especially in the areas near the centerline and close to the walls apparently due to a successful mesh refinement in the sudden expansion section at these zones.

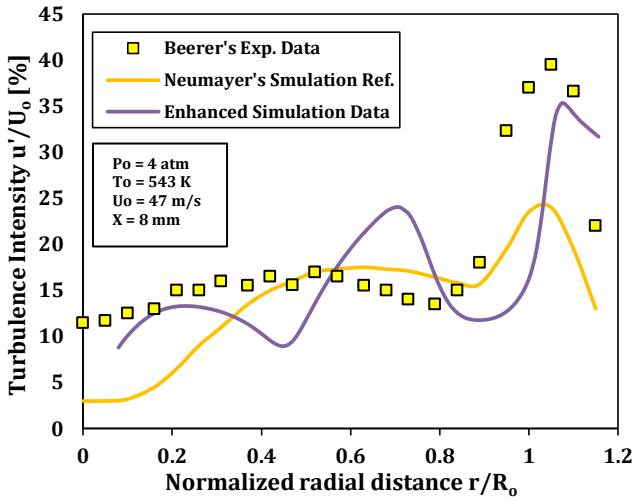

Figure 18: 2D simulation results of turbulence intensity in radial direction

3D Simulation Results

In 3D simulation of non-reacting flow, 3D Large Eddy Simulation (LES) are used to model the turbulence of Low Swirl Injector (LSI). A mesh independence study is conducted to obtain the axial velocity variation in axial direction along the swirler. Unfortunately, no data available for validation of results for both Beerer [5] and Neumayer [6]. To validate the 3D simulation results, the output velocities are used as input data for the non-reacting flow, 2D Reynolds Stress Model (RSM), so it is called here 2D enhanced Simulation.

As described before in the mesh independence study (see "Fig.12."), the mesh step size of 0.25mm is considered suitable for the present case. "Fig. 19." shows axial velocity variation in axial direction along the swirler axial direction for operating pressure of 4 atm., and injector radius R_0 = 19 mm.

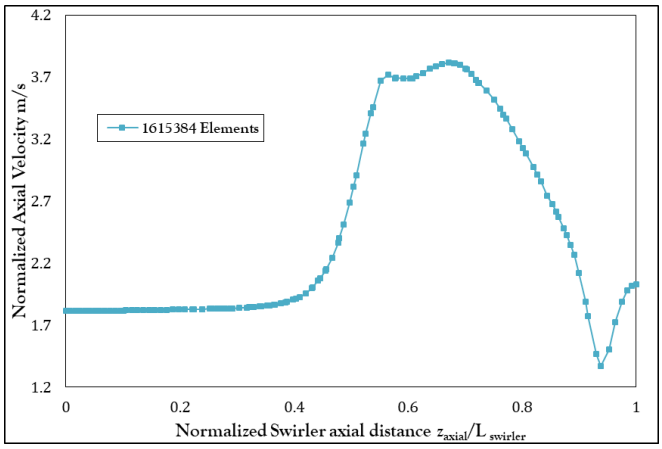

Figure 19: 3D simulation results of axial velocity variation in axial direction

"Figure 20." shows the axial velocity contours for a vertical plane downstream the swirler vanes.

This figure shows the importance of 3-D modeling of the low swirl injector in determining the detailed profile of axial velocity, which will be used in the next set of simulations.

The mean velocities downstream the swirler vanes, which considered the input data for the 2D enhanced simulations, are found as followings:

- Perforated plate outlet mean axial velocity = 25.11 m/s.
- Swirl vanes outlet mean axial velocity = 56.05 m/s.
- Swirl vanes outlet mean tangential velocity = 51.48 m/s.

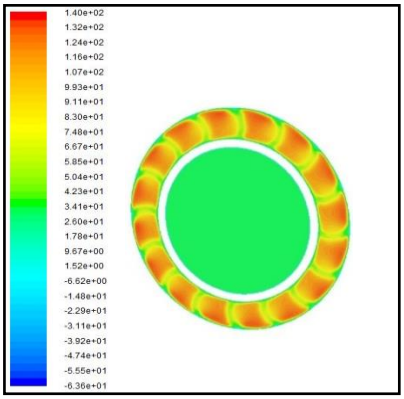

Figure 20: Contours of axial velocity of vertical plane downstream the swirler vanes

2D Enhanced Simulation Results

"Figure 21." shows results of the normalized axial velocity profile in radial direction for enhanced simulation. As mentioned before the enhanced simulation is conducted using the 3D non-reacting flow Large Eddy Simulation velocity results from the LSI as input parameters of the 2D non reacting, RSM simulation for the entire domain of the numerical model.

The enhanced simulation data is compared to both Beerer's experimental data [5] and Neumayer's Simulation [6] with same operating conditions. The operating pressure = 4 atm. Axial velocity profile in radial direction is obtained at 8 mm downstream the sudden expansion. The injector radius R_0 = 19 mm and average velocity in injector U_0 = 47m/s.

The figure shows more qualitative resemblance of present data to Beerer's experimental data [5] in comparison with Neumayer's Simulation [6], especially within range (0 to 0.15) of normalized radial distance. The enhanced 2D data shows some improvement over the 2D simulation data, (see "Fig. 16."), in this range of normalized distance.

It should be mentioned here that the computational time using the present technique of enhanced 2D simulation is recorded not to exceed almost 5 % of computational time for any corresponding simulation using 3D Large Eddy Simulation for the entire model domain.

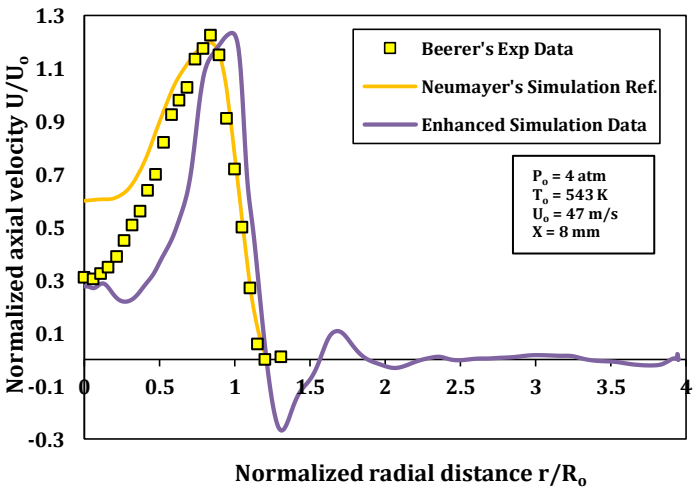

Figure 21: 2D enhanced simulation result of axial velocity profile in radial direction

"Figure 22." shows the axial velocity variation along the centerline after the sudden enlargement of enhanced simulation result. The operating pressure = 8.1 atm., injector radius R_0 = 19mm, using the velocity components results from 3D LES as input data.

The simulated data in this figure is compared only to Beerer's experimental data [5]. Neumayer's Simulation [6] is not included as the numerical data inputs do not match. The present simulation data apparently qualitatively follow experimental data.

The figure indicates that the normalized axial velocity results indicate a closer agreement to the experimental data better than the 2D Simulation (see "Fig. 17.") within the axial distance after the sudden expansion, in the range 4 to 15mm.

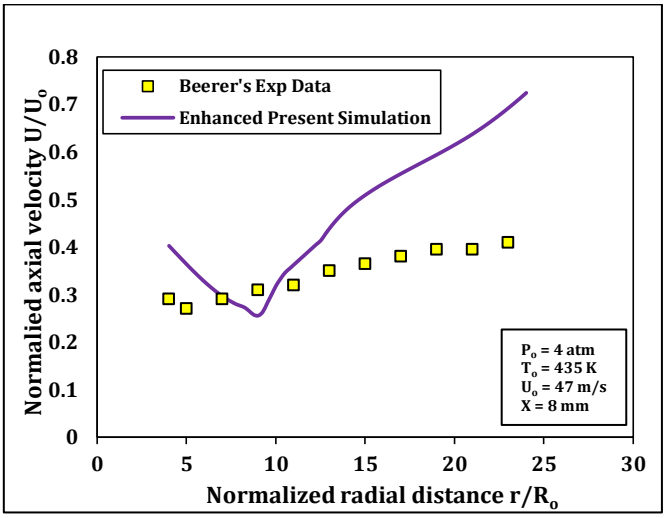

Figure 22: 2D enhanced simulation results of axial velocity variation along the centerline of swirler

"Figure 23." shows the turbulence intensity profile in radial direction for 2D enhanced simulation results. (Operating pressure = 4 atm. at 8mm downstream the sudden expansion and average velocity in injector U_0 = 47m/s). The simulation data is compared with both Beerer's experimental data [5] and Neumayer's Simulation [6] at same operating conditions.

In this figure, the enhanced simulation results of turbulence intensity shows quality improvement over the 2D simulation results and Neumayer's Simulation [6] (see "Fig. 18."), but only within the ranges of normalized radial distance (r/R_O) = (0.08 to 0.35) and (0.9 to 1.2).

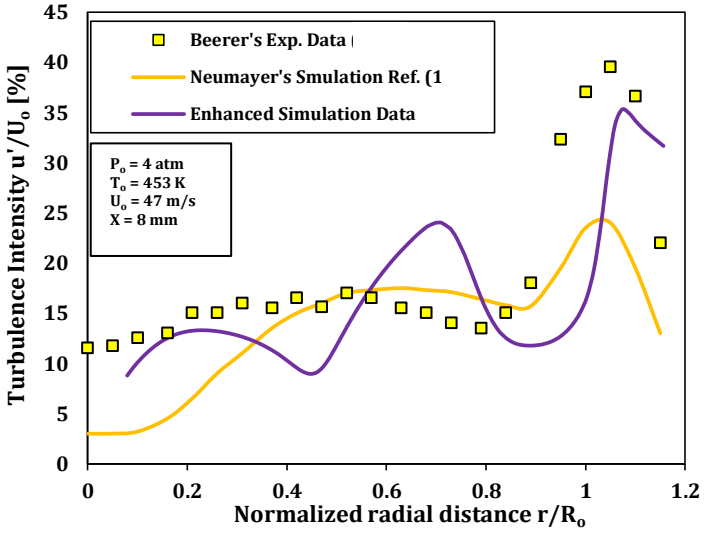

Figure 23: 2D enhanced simulation result of turbulent intensity

However, the previous figures of the 2D enhanced simulation results show some improvement over the 2D simulation data in general, especially for the zones near the centerline or the sudden expansion. Therefore, considered a step forward toward a more accurate solution, in which only 5% of the computational time required for 3D large eddy simulation over the entire domain.

Conclusions

The hypothesis of combining the 2D with 3D simulations in a hope to obtain relatively more suitable values found to be promising.

In comparison with the experimental data, the 2D simulation results showed some improvement for the simulation data but only for some parts of the entire range of experimental data.

There is an improvement of axial velocity in radial direction especially near the centerline of the combustor, also for turbulence intensity along the radial direction the enhanced method show remarkable improvement over wide range of the radial direction. However, for axial velocity along the axial distance after the sudden expansion no significant improvement for the enhanced method.

References

[1]. Zeldovich J. The oxidation of nitrogen in combustion and explosions. Acta Physicochimica (1946); 21(4):577–628.

[2]. Chen C.K., Lau K.S., Chin W.K. Freely propagating open premixed turbulent flames stabilized by swirl. In: 23rd Symposium on combustion; 1992. p. 511-8.

[3]. Cheng R.K., Yehian D.T., Miyatso M.M. Scaling and development of swirl burners for low emission furnace and boilers. Proc Combust Inst 2000; 28: 1305-13.

[4]. Johnson M.R., Littlejohn D., Nazeer W.A., Smith K.O., Cheng R.K. A comparison of the flow fields and emissions of high-swirl injectors and low-swirl injectors for lean premixed gas turbines. Proc Combust Inst 2004; 30 (2005): 2867-74.

[5]. Beerer D.J. Combustion Characteristics and Performance of Low-Swirl Injectors with Natural Gas and Alternative Fuels at Elevated Pressures and Temperatures. PHD Dissertation, University of California, Irvine, USA, 2013.

[6]. Neumayer M. RANS simulation of methane combustion in a Low Swirl. Thesis. Technische Universität München, Munich, Germany, April 2013.

[7]. Launder B.E. Second-Moment Closure and Its Use in Modeling Turbulent Industrial Flows. International Journal for Numerical Methods in Fluids.9. 963–985. 1989.

[8]. Launder B.E., Spalding D.B. The Numerical Computation of Turbulent Flows. Computer Methods in Applied Mech. And Eng., Vol. 3, 269-289, 1974.

[9]. Launder B.E., Reece G.J., Rodi W. Progress in the Development of a Reynolds-Stress Turbulence Closure. J. Fluid Mech. 68(3). 537–566. April 1975.

[10]. Lien F.S., Leschziner M.A. Assessment of Turbulent Transport Models Including Non-Linear RNG Eddy-Viscosity Formulation and Second-Moment Closure. Computers and Fluids. 23(8). 983–1004.1994.

[11]. Sarkar S., Balakrishnan L. Application of a Reynolds-Stress Turbulence Model to the Compressible Shear Layer. ICASE Report 90-18NASA CR 182002. 1990.

[12]. Strahman J.G. Flame Stability of an Ultra-Lean Premixed Low-Swirl Burner. Carleton University. 2007.

[13]. Graham E. B. Analysis of Blowoff in a Low-Swirl Burner: Effects of Burner Geometry and Fuel Composition. Master of Science thesis, Carleton University, Ottawa, Ontario, Canada. November, 2011.